Second-moment interatomic potential for gold and its application to molecular-dynamics simulations

2004 J. Phys.: Condens. Matter 16 8399

(http://iopscience.iop.org/0953-8984/16/46/025)

INSTITUTE OF PHYSICS PUBLISHING JOURNAL OF PHYSICS: CONDENSED MATTER

J. Phys.: Condens. Matter **16** (2004) 8399–8407 PII: S0953-8984(04)81043-9

Second-moment interatomic potential for gold and its application to molecular-dynamics simulations

H Chamati[1] **and N I Papanicolaou**[2]

[1] Institute of Solid State Physics, 72 Tzarigradsko Chaussée, 1784 Sofia, Bulgaria
[2] Department of Physics, Solid State Division, University of Ioannina, PO Box 1186, GR-45110 Ioannina, Greece

E-mail: chamati@issp.bas.bg and nikpap@cc.uoi.gr

Received 20 May 2004
Published 5 November 2004
Online at stacks.iop.org/JPhysCM/16/8399
doi:10.1088/0953-8984/16/46/025

Abstract

We have obtained a new interatomic potential for Au in the framework of the second-moment approximation to the tight-binding model by fitting the total energy of the metal as a function of the volume computed by first-principles calculations. The scheme was validated by calculating the bulk modulus, elastic constants, vacancy formation energy and relaxed surface energies of Au, which were found to be in fair agreement with experiment. We also have performed molecular-dynamics simulations at various temperatures and we have determined the temperature dependence of the lattice constant, mean-square displacements, as well as the phonon density of states and the phonon dispersion curves of the metal. The agreement with the available experimental data is much better than previous works based on the same approximation.

1. Introduction

The application of *ab initio* methods for atomistic simulations of materials is restricted to a short time scale and a few hundreds of atoms in spite of increasing computer speeds. In order to simulate larger systems (up to 10^7–10^8 particles) and longer time scales, empirical and semi-empirical interatomic potentials are found to be very useful. They include many-body terms that are meant to take into account the local electronic density. Among several many-body potentials, the most popular are the embedded atom model (EAM), the Finnis-Sinclair potentials (FS) and the tight-binding (TB) potential in the second moment approximation (SMA). Although based on different approaches, these models share some common features (see e.g. [1]). Despite their simplicity, in many cases, these potentials provide a good and quick description of the physical behaviour of metallic systems. For this reason, they should play a supplementary role to other more accurate techniques.

In the SMA scheme [2–4], the total cohesive energy of the system consists of a band term, proportional to the square root of the second moment of the density of states (DOS) [5], and a repulsive pair-potential term which contains the non-band-structure parts of the energy, such as electrostatic and exchange–correlation interactions. The SMA expression of the total energy is based on a small set of empirical parameters that are usually determined by matching with experimental data, including the cohesive energy, lattice constant (by a constraint on the atomic volume), bulk modulus and independent elastic constants of the system in the appropriate crystal structure at the ground state [6]. The extension of the range of the potential includes interaction up to the fifth neighbours, which provide better and more accurate results compared to experimental information (see [6, 7] and references therein).

The above-mentioned approach has been applied to model the interaction in noble metals [6, 7]. While for Cu and Ag, the agreement achieved for the calculated quantities compared to the experimental measurements was very good, the results for gold were very poor. The vacancy formation energy and the surface energies are considerably lower than the experimental values. Furthermore, the thermal expansion and mean-square displacements are overestimated, while the melting point is anticipated. Moreover, the cutoff phonon frequency is underestimated and the phonon DOS of the metal is too narrow, compared to the experiment. These discrepancies were attributed to the failure of SMA for Au [6, 7].

The aim of the current work is to present a new interatomic potential within the SMA of the tight-binding theory, which provides better agreement with experiment than the previous models [6, 7] for the above-mentioned quantities. Our approach is similar to that of Kallinteris *et al* [7]; that is, in order to obtain the necessary parameters, we adjust the total-energy expression of the SMA to first principles total-energy calculations as a function of the lattice constant. The difference is that in the present scheme we have used a wider lattice constant grid than that used in [7]. We tested the quality of our parameters by computing the bulk modulus, elastic constants, vacancy formation, and surface energies. Furthermore, we performed molecular-dynamics (MD) simulations at various temperatures, obtaining the temperature dependence of the lattice constant and the mean-square-displacements (MSD) as well as the phonon DOS and the phonon dispersion curves along the high-symmetry vectors. The results originating from simulations are compared to the available experimental quantities and to the values of previous models in the SMA approach [6, 7], as well as the recently proposed modified embedded atom potential (MEAM) [8] based on 14 parameters including three experimental values.

The paper is organized as follows: in section 2, we describe the computational method, while the results and their comparison with experimental data are discussed in section 3. Finally, our conclusions are drawn in section 4.

2. Computational methodology

The electronic band structure of Au was calculated by the symmetrized APW method in the muffin-tin approximation [9]. The self-consistent semirelativistic calculations yielded the crystal potential, charge density and eigenvalue sum, which were used in Janak's expression for the total energy [10]. The exchange and correlation interactions were treated by the Hedin–Lundqvist formalism [11]. The computations were performed for both the fcc and bcc structures of the considered metal. A mesh of 89 **k** points in the irreducible Brillouin zone for the fcc and 55 **k** points for the bcc structure was used. The total energy was evaluated for five different lattice parameters for each structure and the resulting variation was fitted to a parabolic function [12].

In the present work, we choose a tight-binding potential in the second moment approximation, according to which the total energy of the system can be expressed as

$$E = \sum_i \left[\sum_{j \neq i} A \, \mathrm{e}^{-p(r_{ij}/r_0 - 1)} - \xi \sqrt{\sum_{j \neq i} \mathrm{e}^{-2q(r_{ij}/r_0 - 1)}} \right], \tag{1}$$

where the first sum over j is a Born–Mayer type pairwise potential adapted for the description of the repulsive contributions, while the second one represents the band-structure term. In the above expression (1), r_{ij} is the distance between atoms i and j, while the interactions up to the fifth neighbours were taken into account. The parameter r_0 is taken to be equal to the nearest-neighbour distance in equilibrium as calculated by the APW method, while the adjustable free parameters A, ξ, p and q in this approach have been determined by fitting to the total energy of the system as computed by first-principles APW calculations as a function of the lattice constant for both the fcc and bcc structures. We used the total energies for both fcc and bcc structures, since it was found that the agreement with the experimental values for the elastic constants was better than the one obtained when using only the fcc structure [13]. The fitting procedure was performed with the aid of the MERLIN package, which provides several minimization algorithms [14]. It should be noted that before performing the fitting procedure, we uniformly shifted the computed total APW energies so that they match, at the minimum of the fcc structure at 0 K, the experimental cohesive energy of Au (3.78 eV [15]).

Using the above interatomic potential, we performed MD simulations in the canonical (NVT) ensemble in order to validate the model at various temperatures. The system is made up of 4000 atoms arranged on an fcc lattice. The simulation box contained 40 atomic layers with 100 atoms each, in which the periodic boundary conditions were imposed in the three space directions. The equations of motion were integrated by means of the Verlet algorithm and a time step $\delta t = 5 \times 10^{-15}$ s. The system was equilibrated at the desired temperature during 1000 integration time steps (5 ps), which were sufficient to obtain stationary values for the kinetic and potential energies. The thermodynamic averages were computed satisfactorily over 50 ps trajectories. The vacancy formation and the surface energies were calculated at $T = 0$ K by using a quasidynamic minimization procedure. The free surfaces were produced by fixing the dimensions of the computational box at a length twice as large as the thickness of the crystal along the direction normal to the surface; an infinite slab was thus constructed delimited by two free surfaces parallel to (100), (110) or (111) planes. The above length is enough to avoid interactions between the periodic slabs and, in addition, the number of occupied atomic layers is sufficient to reproduce bulk-like properties in its central part.

The value of the lattice constant at each temperature was chosen so as to result in zero pressure in the system, while the atomic mean-square displacements were determined on a layer-by-layer basis from equilibrium averages of the atomic density profiles. Finally, the phonon DOS was obtained from the Fourier transform of the velocity autocorrelation function and the spectral densities were calculated by Fourier-transforming the velocity- and position-dependent autocorrelation function for a given polarization and a specific $\mathbf{k}$ vector in the Brillouin zone. Consequently, the phonon-dispersion curves were deduced from frequencies found in the corresponding spectral densities. In particular, we used a mesh of 20 $\mathbf{k}$ vectors along each symmetry direction and then we performed a cubic spline interpolation.

3. Results and discussion

In figure 1, we plot the opposite of the computed cohesive energies of Au as a function of the volume in the fcc and bcc structures (solid lines) after the appropriate energy shift, as

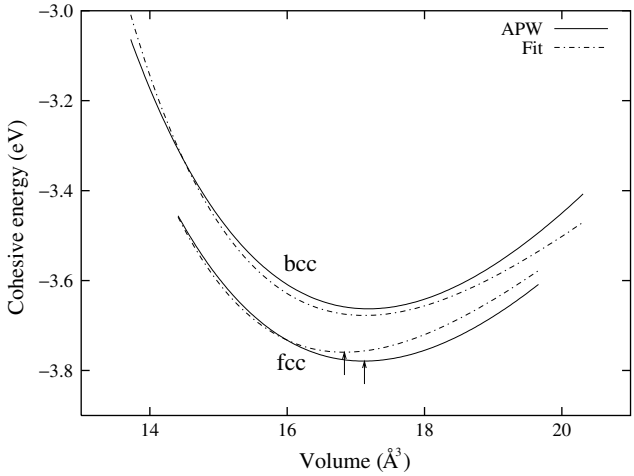

Figure 1. Volume dependence of the calculated cohesive energies of Au from APW (solid line) and the results of the fitting procedure (dot-dashed line). The arrows indicate the locations of the minima of APW and fitting curves.

Table 1. Potential parameters of equation (1) deduced by fitting to the calculated cohesive energy as a function of the volume, along with the corresponding values in [6, 7].

	ξ (eV)	A (eV)	q	p	r_0 (Å)
Present work	1.32795	0.08170	3.12572	14.6027	2.89267
Parameters [6]	1.790	0.2061	4.036	10.229	2.8843
Parameters [7]	10.9249	13.5959	2.7381	6.3469	1.7517

Table 2. Calculated and experimental [17] lattice constants, along with the cohesive energies [15] for Au.

		Calculated		
	Experimental	Present work	SMA [6]	SMA [7]
a_0 (Å)	4.07	4.068	4.079	4.06
E_0 (eV atom^{-1})	3.78	3.76	3.779	3.77

discussed in section 2. The result of the fitting procedure (dot-dashed line) is presented in the same figure. From this adjustment, we have determined the values of the parameters of equation (1), which are presented in table 1, together with those of [6, 7]. In table 2, we report results for the calculated equilibrium lattice constants and cohesive energies within the present TB-SMA along with those of [6, 7] in comparison with experiment. The equilibrium lattice constant calculated by the APW method was 4.09 Å, while the corresponding value of the fitted SMA was 4.068 Å. The parameters have been used to calculate the bulk modulus, using the method proposed in [12]. The elastic constants of Au were calculated at the lattice constant corresponding to the lowest potential energy following the method of Mehl *et al* [16]. In table 3, we report these calculated values, those in [6–8] and the corresponding experimental values [17]. Our values for the bulk modulus B and elastic constant C_{12} are in good agreement

Table 3. Computed properties of Au along with experimental, SMA results [6, 7] and MEAM results [8].

		Calculated			
	Experimental	Present work	SMA [6]	SMA [7]	MEAM [8]
Lattice properties					
B (10^{11} Pa)	1.69[a]	1.835	1.65	1.69	1.803
C_{11} (10^{11} Pa)	1.89[a]	2.36	1.87	1.84	2.015
C_{12} (10^{11} Pa)	1.593[a]	1.56	1.54	1.61	1.697
C_{44} (10^{11} Pa)	0.42[a]	1.011	0.45	0.28	0.454
Vacancy					
E_v^f (eV)	0.94[b]	1.402	0.75	0.49	0.90
Surfaces					
$\gamma_s(110)$ (J m^{-2})	1.50[c]	1.198	0.626[d]	0.45	1.179
$\gamma_s(100)$ (J m^{-2})	1.50[c]	1.056	0.58[d]	0.44	1.138
$\gamma_s(111)$ (J m^{-2})	1.50[c]	0.939	0.493[d]	0.37	0.928
Phonon frequencies					
$\nu_L(X)$ (THz)	4.61[e]	5.05	3.20	3.16[f]	
$\nu_T(X)$ (THz)	2.75[e]	3.50	1.51	1.97[f]	
$\nu_L(L)$ (THz)	4.70[e]	5.00	3.24	2.93[f]	
$\nu_T(L)$ (THz)	1.86[e]	2.36	2.27	1.31[f]	

[a] From [17].
[b] From [19].
[c] From [20].
[d] These values are computed for this paper using the parameters of the potential from [6].
[e] From [25].
[f] These values are computed for this paper using the parameters of the potential from [7].

with experimental measurements [17], the TB method of Mehl and Papaconstantopulos [18] and those of MEAM reported in [8], while the disagreement for the C_{11} is about 25%. Moreover, there is an important discrepancy for C_{44}. It should be noted that the values in [6] are very close to the experimental elastic constants, since their potential was fitted to those quantities.

We have determined the vacancy formation energy, using the quasidynamic minimization method and the procedure described in section 2. The result for this quantity, after relaxation of the whole system, is given in table 3 along with the experimental value [19]. The result predicted by TB-SMA is higher than the experimental value and those in [6–8]. We have also computed the relaxed surface energies of low index surfaces (100), (110) and (111). A comparison of these results to the experiment in [20] and the reported results in [6–8] is shown in table 3. Notice that the experimental energies are those of polycrystalline surfaces. The calculated surface energies in table 3 are in better agreement with experiment [20] compared to the computed values in [6, 7] and are comparable to the results obtained within the framework of MEAM [8]. Our potential model follows the trends usually found on fcc metallic surfaces: the largest surface energy is that of the (110) face, while the smallest one is that of the (111) face. These results are compatible with the experimental data [21] since we have found the ratio $\gamma_s(110)/\gamma_s(100) = 1.13$ in good agreement with the experimental value of 1.11 and the ratio $\gamma_s(110)/\gamma_s(111) = 1.28$ compared to the experimental one of 1.25.

In the following, we present some finite-temperature results for various structural and thermal properties. In figure 2, we present the thermal expansion of Au as a function of temperature, deduced from our MD simulations along with the corresponding experimental

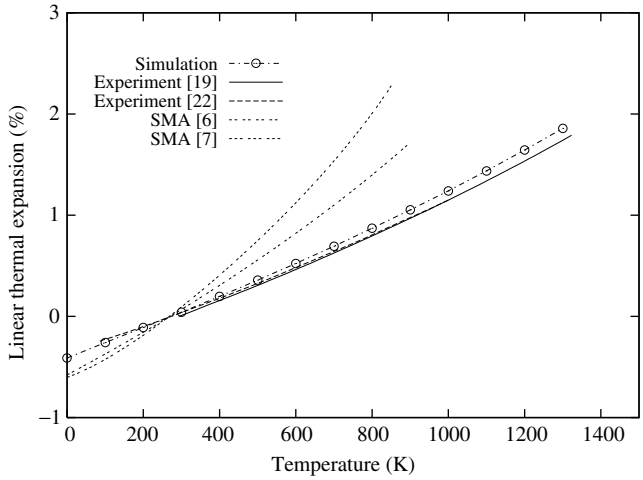

Figure 2. Temperature dependence of the lattice expansion for Au. The experimental results are taken from [19, 22].

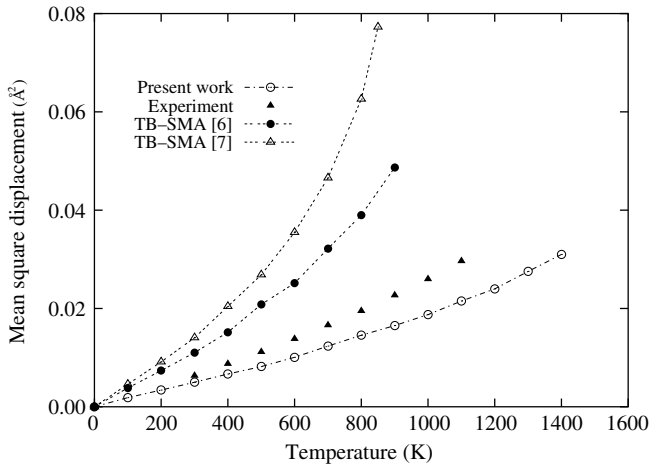

Figure 3. Mean-square displacements of bulk Au as a function of the temperature, compared to the experimental values of [23] and the results obtained using the TB-SMA potential of [6, 7].

values [19, 22] and the respective data in [6, 7]. It is obvious that the agreement of our factors with the experimental ones is excellent and much better than the results in [6, 7]. The linear expansion coefficient at 0–100 K is found to be $1.4 \times 10^{-5}\,\mathrm{K}^{-1}$ to be compared to the experimental value of $1.4 \times 10^{-5}\,\mathrm{K}^{-1}$ [15] and the calculated value of $1.42 \times 10^{-5}\,\mathrm{K}^{-1}$ for MEAM [8], as well as those of $2.3 \times 10^{-5}\,\mathrm{K}^{-1}$ obtained using the model of Cleri and Rosato [6] and $2.4 \times 10^{-5}\,\mathrm{K}^{-1}$ of Kallinteris *et al* [7].

In figure 3, we compare the temperature dependence of our computed atomic MSDs (open circles) with experimental data (filled triangles) [23] and results obtained with the model proposed in [6] (filled circles) and [7] (open triangles). Our results are lower than the experimental values, but more accurate than those obtained by the SMA method in [6, 7]. According to Lindemann's criterion [24], the melting point can be empirically estimated by

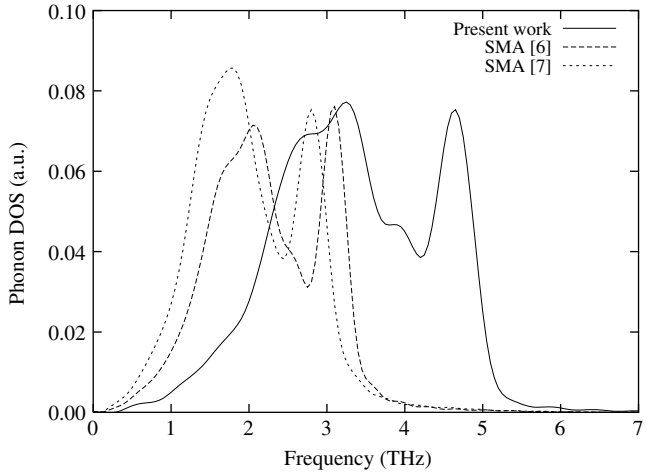

Figure 4. Phonon DOS of Au (in arbitrary units) at 300 K deduced from the present MD simulations along with the results obtained using the TB-SMA potential of [6, 7].

the MSD values. In our case, it is found to be 1630 K; therefore, it is clear that the present model results in a higher value for the temperature of melting, compared to the experimentally measured value of 1338 K [15] and the result of 1410 K obtained with the MEAM of Lee *et al* [8], while previously proposed models [6, 7] gave an important underestimation of the melting point (about 850 K).

In figure 4, we present the calculated phonon DOS at room temperature obtained by performing MD simulations. We observe that the main features of the phonon frequency spectrum are well reproduced. The shape of the curve is smooth as a consequence of the use of the velocity autocorrelation function. Comparing our phonon DOS with previous works based on the TB-SMA potentials [6, 7], we find that our results are superior since the cutoff frequency is closer to the experimental one [25] and the width of the phonon spectrum is comparable to the corresponding one from experiment, while the parameters in [6, 7] produce a narrow spectrum. In table 3, we compare our calculated results for the transverse as well as the longitudinal branches of the frequencies $\nu(X)$ and $\nu(L)$ at the borders of the Brillouin zone to the experimental [25] and the SMA results in [6, 7]. It is clear that our results are more accurate than those of the SMA approach in [6, 7].

The phonon-dispersion curves are displayed in figure 5 together with the experimental results obtained using inelastic scattering techniques [25]. The main trends of the phonon-dispersion branches are reproduced, but there is a slight disagreement at small q, especially for transverse modes, due to the discrepancy in the elastic constants. Moreover, there is a slight overestimation of the cutoff frequency in the Brillouin-zone boundaries. This is compatible with the inaccuracy found in our calculated value of C_{44} and the late melting of the system.

4. Conclusions

We presented an interatomic potential of Au within the SMA of TB theory by adjusting the parameters of the energy functional to first-principles total energy as a function of the volume. The resulting model potential was used to compute the bulk modulus, elastic constants, vacancy formation and surface energies. Our theoretical predictions show satisfactory accuracy except

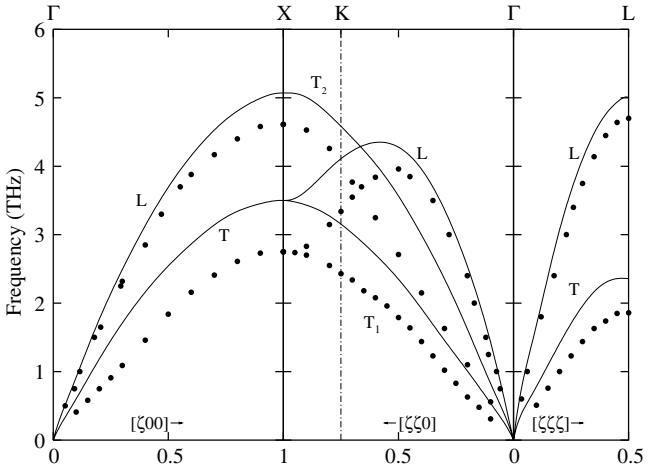

Figure 5. Phonon dispersion curves of Au at 300 K along high-symmetry directions. Solid lines correspond to MD simulations after a cubic spline interpolation. The filled circles refer to the measured data from [25].

for the elastic constant C_{44}. The calculated surface energies are in better agreement with measurements than the computed values of previous SMA models and, in addition, show the correct experimental anisotropies.

Finite temperature MD simulations were used to deduce the temperature dependence of the thermal lattice expansion and the mean-square displacements as well as the phonon DOS and the phonon-dispersion curves. The predicted values are in acceptable agreement compared to the experimental results. It should be noted that the present SMA model provides much better accuracy for the determination of the above quantities compared to the previously proposed SMA potentials. We conclude that the current potential can be useful in long simulations for the determination of the related physical properties of gold systems such as epitaxial growth, surface diffusion, island formation, nanostructures and thermal properties. However, it is expected to fail in describing the liquid phase for temperatures slightly higher than the melting temperature.

Notice that despite the relatively simple form of the potential and the small number of parameters used to fit the total energy, the potential we present here has shown its ability to reproduce quite well some experimental results and has a comparable weight as the recently proposed MEAM potential [8], where 11 parameters are used to fit the total energy.

References

[1] Voter A F 1994 The embedded-atom model *Intermetallic Compounds* vol 1 *Principles* ed J H Westbrook and R L Fleischer (New York: Wiley)
[2] Ducastelle F 1970 *J. Phys.* (Paris) **31** 1055
[3] Gupta R P 1981 *Phys. Rev.* B **23** 6265
[4] Tomanek D, Aligia A A and Balseiro C A 1985 *Phys. Rev.* B **32** 5051
[5] Sutton A P 1994 *Electronic Structure of Materials* (Oxford: Oxford University Press)
[6] Cleri F and Rosato V 1993 *Phys. Rev.* B **48** 22
[7] Kallinteris G C, Papanicolaou N I, Evangelakis G A and Papaconstantopoulos D A 1997 *Phys. Rev.* B **55** 2150
[8] Lee B-J, Shim J-H and Baskes M I 2003 *Phys. Rev.* B **68** 144112
[9] Mattheiss L F, Wood J H and Switendick A C 1968 *Methods Comput. Phys.* **8** 63

[10] Janak J F 1974 *Phys. Rev.* B **9** 3985
[11] Hedin L and Lundqvist B I 1971 *J. Phys. C: Solid State Phys.* **4** 2064
[12] Birch F 1978 *J. Geophys. Res.* **83** 1257
[13] Sigalas M M and Papaconstantopoulos D A 1994 *Phys. Rev.* B **49** 1574
[14] Papageorgiou D G, Demetropoulos I N and Lagaris I E 1998 *Comput. Phys. Commun.* **109** 227
[15] Kittel C 1996 *Introduction to Solid State Physics* (New York: Wiley-Interscience)
[16] Mehl M J, Klein B M and Papaconstantopoulos D A 1994 *Intermetallic Compounds* vol 1 *Principles* ed J H Westbrook and R L Fleischer (New York: Wiley)
[17] Simmons G and Wang H 1971 *Single Crystal Elastic Constants and Calculated Aggregate Properties: A Handbook* 2nd edn (Cambridge, MA: MIT Press)
[18] Mehl M J and Papaconstantopulos D A 1996 *Phys. Rev.* B **54** 4519
[19] Simmons R O and Balluffi R W 1962 *Phys. Rev.* **125** 862
[20] Tyson W R and Miller W A 1977 *Surf. Sci.* **62** 267
[21] Hamelin A and Lecoeur J 1976 *Surf. Sci.* **57** 771
[22] Nix F C and MacNair D 1941 *Phys. Rev.* **60** 597
[23] Killean R C G and Lisher E J 1975 *J. Phys. F: Met. Phys.* **5** 1407
[24] Lindemann F A 1910 *Phys. Z.* **11** 609
[25] Lynn J W, Smith H G and Nicklow R M 1973 *Phys. Rev.* B **8** 3493